Enhancement of peak intensity in a filament core with spatiotemporally focused femtosecond laser pulses

Bin Zeng,[1,3] Wei Chu,[1,3] Hui Gao,[2] Weiwei Liu,[2,*] Guihua Li,[1,3] Haisu Zhang,[1,3] Jinping Yao,[1] Jielei Ni,[1,3] See Leang Chin,[4] Ya Cheng,[1,†] and Zhizhan Xu[1,‡]

[1]*State Key Laboratory of High Field Laser Physics, Shanghai Institute of Optics and Fine Mechanics, Chinese Academy of Sciences, Shanghai 201800, China*

[2]*Institute of Modern Optics, Nankai University, Tianjin, 300071 China*

[3]*Graduate School of Chinese Academy of Sciences, Beijing 100080, China*

[4]*Center for Optics, Photonics and Laser (COPL) and Department of Physics, Engineering Physics and Optics, Université Laval, Québec City, QC, Canada, G1V 0A6*

(Received 8 September 2011; published 7 December 2011)

We demonstrate that the peak intensity in the filament core, which is inherently limited by the intensity clamping effect during femtosecond laser filamentation, can be significantly enhanced using spatiotemporally focused femtosecond laser pulses. In addition, the filament length obtained by spatiotemporally focused femtosecond laser pulses is ∼25 times shorter than that obtained by a conventional focusing scheme, resulting in improved high spatial resolution.

DOI: 10.1103/PhysRevA.84.063819 PACS number(s): 42.65.Re, 42.68.Ay, 42.68.Wt

I. INTRODUCTION

Due to the potential applications in the fields of remote sensing, pulse compression, coherent light conversion, and THz generation, femtosecond filamentation has attracted broad attention since its discovery and become a subject under intensive investigation in recent years [1–6]. During filamentation, femtosecond pulses can propagate tens of meters to several kilometers in the atmosphere without significantly losing peak intensity [7–9], owing to the dynamic interplay between self-focusing induced by the optical Kerr effect and defocusing of plasma generated through multi-photon-tunnel ionization of the molecules and atoms. This dynamic balance results in relatively stable peak intensity typically in the range of 10^{13}–10^{14} W/cm^2 depending on the focusing condition in the filament core in air due to the well-known intensity clamping effect [10–15]. The intensity clamping effect has profound implications for applications of filamentation in nonlinear optical research. On the one hand, the highly stable intensity clamped in the filament core will significantly reduce the fluctuation of femtosecond laser intensity [16]; on the other hand, the intensity clamping effect creates a barrier for higher peak intensity achievable in femtosecond laser filamentation. Although improved peak intensity can be obtained in the filament core by use of tight focusing [17,18], under such conditions the filament cannot be launched far away. In this paper we demonstrate, both experimentally and theoretically, that peak laser intensities could be significantly enhanced in the filament core through spatiotemporal manipulation of femtosecond laser pulses [19]. In addition, a ∼4-mm-long filament was produced, which is ∼25 times shorter than that obtained without using the temporal focusing technique. For remote sensing, a shortened filament will lead to not only improved spatial resolution but also enhanced signal-to-noise ratio owing to the reduced white-light generation [5]. This technique can also be useful for other applications in strong field laser physics. As an example, high-order harmonic generation (HHG), which sometimes also suffers from the intensity clamping due to filamentation in the working gas, could benefit from the temporal focusing technique because of the higher achievable peak intensity, thus higher conversion efficiency and higher cutoff photon energies could be attainable. In particular, for HHG experiments employing a loose focusing scheme [20], separation of the high-order harmonics and the pump IR laser beam is usually a tough issue because of the damage of the optics placed downstream from the HHG cell. Temporal focusing could provide a good solution as it effectively reduces the Rayleigh length.

II. EXPERIMENTAL SETUP

The experiment was carried out with a commercial Ti:sapphire laser system (Legend Elite Duo, Coherent, Inc.) which delivers 1 kHz laser pulses at a center wavelength of 800 nm with a spectral bandwidth of ∼30 nm. The experimental setup is illustrated in Fig. 1. The laser pulses were derived directly from the amplifier without compression. Its beam diameter was ∼9 mm ($1/e^2$) and then the beam size was reduced by five times in the horizontal direction using a cylindrical convex lens ($f = 50$ cm) and a cylindrical concave lens ($f = -10$ cm). The laser was dispersed by a parallel pair of 1500 lines/mm gratings in the horizontal direction. The distance between the gratings was set to be ∼73 cm to compensate for the temporal dispersion of different spectral components. After being dispersed by the gratings, the laser beam was ∼40 mm ($1/e^2$) along the dispersed direction. It was then focused with a 100-cm focal length lens into the air. The fluorescence spectrum from N_2 near the focus was measured by a spectrometer (Shamrock 303i, Andor Corp.). Two 5-cm focal length lenses were used in a 4-f geometry to image the fluorescence to the entrance slit of the spectrometer. The width of the entrance slit is 20 μm. A half-wave plate and

*liuweiwei@nankai.edu.cn
†ya.cheng@siom.ac.cn
‡zzxu@mail.shcnc.ac.cn

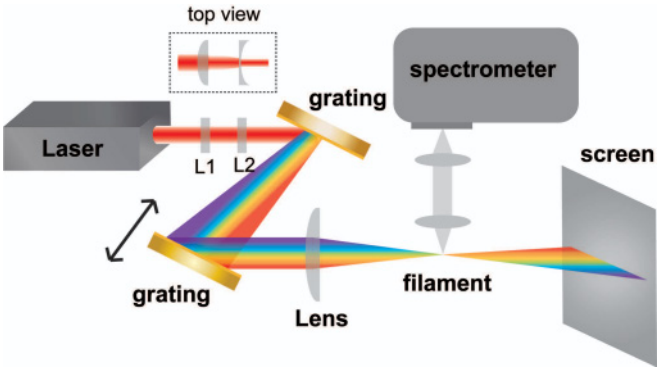

FIG. 1. (Color online) Schematic of the experimental setup.

a Glan-Taylor prism were employed to change the incident energy of the laser pulses. For comparison, the fluorescence spectrum of the filamentation generated without using the spatiotemporal focusing was also measured, i.e., without using the cylindrical lenses. In this case, the pulse duration after compression was ~40 fs.

III. ENHANCEMENT OF PEAK INTENSITY IN FILAMENT CORE USING TEMPORAL FOCUSING

Figures 2(a) and 2(b) show the filament profiles generated with and without the spatiotemporal focusing technique captured by a digital camera (D40, Nikon) from the side of the filaments. When using the 100-cm focal lens to focus the 40-fs laser pulse without spatiotemporal focusing directly, the length of the filament is ~100 mm. However, when the spatiotemporal focusing technique is employed, the length of the filament decreases to less than 4 mm. The shortened filament implies that the peak intensity of the pulse decays quickly away from the focus. The rapid decrease of the peak intensity beyond the focus is caused by two reasons. Firstly, as different spectral components of the beam are separated spatially, only at the focus will all the spectral components converge to form an ultrashort intense pulse, while before or after the focus, different spectral components of the beam diverge spatially resulting in a spatially chirped narrow spectral bandwidth, thus a longer pulse. Secondly, as different spectral components are spatially dispersed, only in the geometric focus is the pulse chirp free, while before (after) the focus the pulse is highly positively (negatively) chirped. The large chirp elongates the temporal pulse duration. Both these two effects ensure that the shortest pulse duration can only be achieved in the focus, while away from the focus, the pulse duration grows quickly. To confirm this, we explore the propagation of the pulses using the linear propagation method. The intensity distribution of the laser after dispersed by the gratings can be written as [19]

$$A_1(x,y,\omega) = A_0 \exp\left[-\frac{(\omega-\omega_0)^2}{\Omega^2}\right] \exp\left\{-\frac{[(x-\Delta x(\omega)]^2}{w_{0x}^2} - \frac{y^2}{w_{0y}^2}\right\}, \quad (1)$$

where A_0 is the field amplitude, ω_0 is the center frequency of the laser, and $\sqrt{2\ln 2}\Omega$ is the full width half maximum (FWHM) of the frequency spectrum of the pulse. $\sqrt{2\ln 2}w_{0x}$ and $\sqrt{2\ln 2}w_{0y}$ are the FWHM of beam sizes in the horizontal and vertical directions, respectively. $\Delta x(\omega)$ describes the displacement of each spectral component. In the calculation, we assume that all the spectral components have the same initial phase. According to the experiment, the spectral bandwidth is set to be 30 nm, and the beam size is 1 and 5 mm in the x and y directions, respectively.

Using the slowly varying envelope approximation, the field after the lens is

$$A_2(x,y,\omega) = A_1(x,y,\omega) \exp\left\{-ik\frac{x^2+y^2}{2f}\right\}. \quad (2)$$

Here $k = 2\pi\omega/c$ and f is the focal length of the lens.

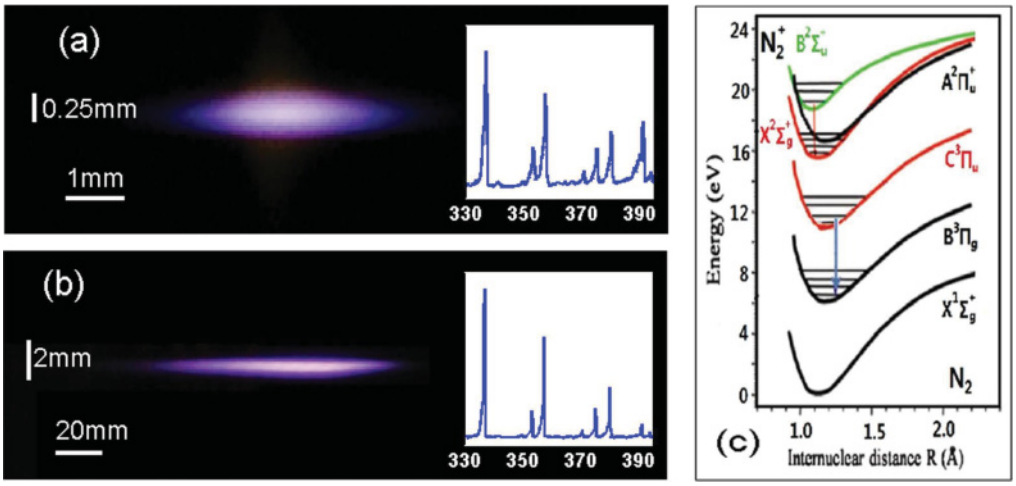

FIG. 2. (Color online) Filamentation profiles captured by a digital camera (a) with and (b) without using spatiotemporal focusing. Please note the scale change from (a) to (b). Insets show the corresponding N_2 fluorescence spectra. (c) Indicates the energy diagram of nitrogen molecule.

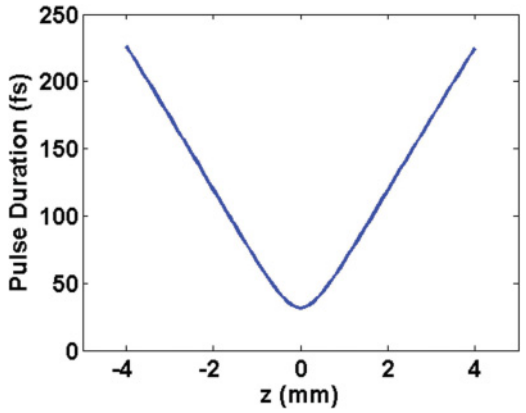

FIG. 3. (Color online) Calculated pulse duration in the vicinity of geometric focus for spatiotemporally focused femtosecond laser pulses.

The laser field near the focus can be calculated using the Fresnel diffraction equation,

$$A_3(x,y,z,\omega) = \frac{e^{ikz}}{i\lambda z}\int\int_{-\infty}^{\infty} A_2(\xi,\eta,\omega)\exp\left\{i\frac{k}{2z}[(x-\xi)^2 + (y-\eta)^2]\right\}d\xi d\eta. \quad (3)$$

The intensity distribution in the time domain can be obtained by performing the inverse Fourier transform of the $A_3(x,y,z,\omega)$,

$$I(x,y,z,t) = |A_3|^2 = \left|\int_{-\infty}^{\infty} A_3(x,y,z,\omega)\exp(i\omega t)\right|^2. \quad (4)$$

The FWHM pulse duration near the focus was shown in Fig. 3. On the other hand, we have known that dispersion-induced lengthening of the pulse could be described by so-called group-velocity-dispersion (GVD) parameter [21]:

$$\tau(z) = \tau_0\sqrt{1+\left(\frac{zk_2}{\tau_0}\right)^2}, \quad (5)$$

where z, $\tau(z)$ denote propagation distance and pulse duration (half width at $1/e^2$), respectively. τ_0 represents the transform limited pulse duration at the focus and k_2 indicates the GVD parameter. The same plot demonstrated in Fig. 3 could be obtained according to Eq. (5) by introducing an effective value of GVD parameter $k_2 = 1.1 \times 10^4$ fs^2/cm, which is roughly five orders of magnitude larger than that in air (0.213 fs^2/cm). Note that since the Rayleigh range (3.9 cm) is much longer than the effective "dispersion" length (0.8 mm), geometrical focusing could be neglected near the focus when deducing the effective value of k_2. The quick increase of the pulse duration leads to a rapid decrease of the peak intensity, resulting in a shorter filament or a shorter zone of high intensity. To investigate the clamped intensity in the filament, we measured the fluorescence of nitrogen molecules and ions generated by focusing the laser beam into the air with a 100-cm focal lens (both with and without spatiotemporal focusing configuration). Two representative spectra are demonstrated by the insets of Figs. 2(a) and 2(b), respectively. Both spectra in the insets feature "continuum free" as reported previously [22]. Particularly, the 337- and 391-nm lines in the spectra can be assigned to the second positive band of $N_2(C\,^3\Pi_u \rightarrow B\,^3\Pi_g)$ and the first negative band system of $N_2^+\left(B\,^2\Sigma_u^+ \rightarrow X\,^2\Sigma_g^+\right)$, respectively [see Fig. 2(c)]. It was revealed that the population of $B\,^2\Sigma_u^+$ state results from the direct ionization of inner valence electrons [5,22–24]. The following (0–0) transition gives rise to the strongest band head of the first negative system at 391 nm. Hence, the 391-nm signal $S_{391\text{nm}}$ is proportional to the ionization probability of direct inner valence electron ionization, experimentally yielding [22,23] $S_{391} \propto N_i^{\text{excited}} \propto I^{n_1}$ or $S_{391} = aI^{n_1}$, where N_i^{excited} denotes the number of ions in the excited state $B\,^2\Sigma_u^+$, n_1 denotes the effective order of nonlinearity of inner valence electron ionization, and a indicates a constant. Recently, Xu *et al.*, have shown that the formation of N_4^+ through $N_2^+ + N_2 = N_4^+$ and the dissociative recombination between N_4^+ and e ($N_4^+ + e \rightarrow N_2^* + N_2$) populates the excited state $C\,^3\Pi_u$ of N_2 [25]. Hence, the fluorescence emission associated with the second positive band system of $N_2(C\,^3\Pi_u \rightarrow B\,^3\Pi_g)$, such as 337 nm, is proportional to the total number of ions. The total number of ions is the sum of the ions in the ground state and in the excited state, the latter through inner valence electron ionization. They are denoted by $N_i^{\text{ground}} + N_i^{\text{excited}}$, respectively. The ground state ions come from the normal ionization of the electron with the lowest ionization potential which results in the generation of ground state ions, N_i^{ground}. We thus have the following relationship:

$$\begin{aligned} S_{391\text{nm}} &= aI^{n_1}, \\ S_{337\text{nm}} \propto N_i^{\text{total}} &= N_i^{\text{excited}} + N_i^{\text{ground}} = aI^{n_1} + bI^{n_2}, \end{aligned} \quad (6)$$

where $S_{337\text{nm}}$ denotes the fluorescence signal at 337 nm, N_i^{total} the total number of ions, N_i^{ground} the number of ions in the ground state, and b is a proportionality constant. Thus,

$$S_{337\text{nm}} = k(aI^{n_1} + bI^{n_2}), \quad (7)$$

where k is a proportionality constant. Finally, we obtain the ratio R between the two fluorescence strengths given by the following:

$$R \equiv \frac{S_{391\text{nm}}}{S_{337\text{nm}}} = \frac{aI^{n_1}}{k(aI^{n_1} + bI^{n_2})} \propto \frac{1}{1+(b/a)I^{n_2-n_1}}. \quad (8)$$

In Fig. 4, we plot the strength ratio ($S_{391\text{nm}}/S_{337\text{nm}}$) as a function of the propagation distance in the vicinity of the geometrical focus when spatiotemporal focusing is applied. Clearly, the ratio is peaked at around $z = 0$, and decreases quickly when the laser pulse is away from the focus, indicating an abrupt change of laser intensity. The results presented in Fig. 4 imply that higher laser intensity will give rise to a larger ratio. It is easily understood by Eq. (8) since $n_2 < n_1$ in view of higher ionization potential of the inner electrons.

Furthermore, Fig. 5 shows the experimentally measured strength ratios of the 391- and the 337-nm lines as a function of the laser energy with and without spatiotemporal focusing. It can be seen that in the case without using spatiotemporal focusing, the ratio shows a first rapid rise with the increase of the input laser energy. While the energy is higher than 1 mJ, the ratio remains almost constant since the peak intensity does not increase due to the intensity clamping. However, when the spatiotemporal focusing technique was employed, the intensity

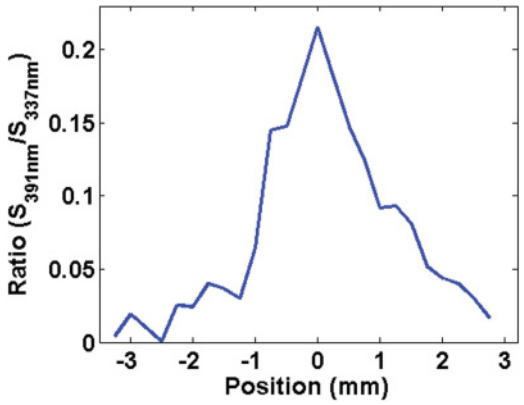

FIG. 4. (Color online) Experimentally measured intensity ratio of 391-nm to 337-nm lines as a function of the propagation distance when using spatiotemporal focusing.

ratio of the 391 nm to the 337 nm first grew with the increase of the incident energy, and then it reached a plateau at ~0.15 when the laser energy is larger than 4.5 mJ. Figure 5 indicates that the intensity clamping occurs at a higher energy level with higher intensity.

IV. NUMERICAL SIMULATION BASED ON NONLINEAR WAVE EQUATION

In order to gain deeper insight into the mechanism behind the enhanced peak intensity in the core of the filament created by a spatiotemporally focused femtosecond laser pulse, we have performed numerical simulations based on the nonlinear wave equation using the slowly varying envelope approximation written in the retarded coordinate system $\tau = t - z/v_g(\omega)$ as [1–4]:

$$2ik_0\frac{\partial A}{\partial z} + \Delta_\perp A + 2\left(1 + \frac{i}{\omega}\frac{\partial}{\partial t}\right)\frac{k_0^2}{n_0}(\Delta n_{\text{Kerr}} + \Delta n_{\text{plasma}})A - k_2 k_0\frac{\partial^2 A}{\partial \tau^2} - ik_0\alpha A = 0. \quad (9)$$

Equation (9) involves a number of optical effects such as diffraction, self-focusing, group-velocity dispersion, and self-steepening as well as plasma generation and energy losses due to multi-photon-tunnel ionization. Here, A is the electric field envelope function. $v_g(\omega), k_0, k_2$ and α represent group velocity, wave number, group velocity dispersion parameter, and absorption coefficiency associated with ionization in air, respectively. Their values are adapted from Ref. [26]. It is worth mentioning that Brabec and Krausz have pointed out that the space-time focusing plays a non-negligible role when the pulse duration is approaching the single cycle limit (for 800 nm, it is 2.67 fs) [27]. Though generation of a single cycle pulse in noble gas cell has been observed by elaborate gas pressure control [28,29], the shortest pulse length obtained through self-compression of filamentation in air is significantly longer than this limit [30]. Hence, we consider that the model of Eq. (9) can capture the major features of the nonlinear propagation in air. The nonlinear contribution to the refractive index from the neutral molecules is considered in the form [31,32]

$$\Delta n_{\text{Kerr}}(t) = n_2\left\{|A(t)|^2 + \int_{-\infty}^{t} H(t-t')\left|A(t')\right|^2 dt'\right\}, \quad (10)$$

where n_2 is the nonlinear index of refraction. The delayed Raman response function $H(t)$ was approximated based on the damped model by the following equation:

$$H(t) = \frac{1}{T_k}\theta(t)\exp(-t/T_k), \quad (11)$$

where $\theta(t)$ is the Heaviside function and the fitting parameter $T_k = 70$ fs [33]. The refraction index change due to plasma can be approximated as

$$\Delta n_{\text{plasma}} = -\frac{\omega_p^2}{2\omega_0^2}. \quad (12)$$

Here the plasma frequency is given by

$$\omega_p = \sqrt{\frac{4\pi e^2}{m_e}N_e}, \quad (13)$$

where e and m_e correspond to the charge and mass of the electron and N_e denotes the plasma density. Plasma generation through multi-photon-tunnel ionization of N_2 and O_2 is taken into account via fitting the ionization rates by the experimental data for the relevant laser intensity range [24]. In details, the total plasma density is given rise by the ionization of N_2 and O_2:

$$\frac{dN_e}{dt} = \frac{dN_{e,\text{N}_2}}{dt} + \frac{dN_{e,\text{O}_2}}{dt}, \quad (14)$$

where

$$\frac{dN_{e,\text{N}_2}}{dt} = \left(N_{0,\text{N}_2} - N_{e,\text{N}_2}\right)R_{\text{N}_2}\left(\frac{I}{I_T}\right)^{\alpha_{\text{N}_2}},$$
$$\frac{dN_{e,\text{O}_2}}{dt} = \left(N_{0,\text{O}_2} - N_{e,\text{O}_2}\right)R_{\text{O}_2}\left(\frac{I}{I_T}\right)^{\alpha_{\text{O}_2}}. \quad (15)$$

In Eq. (15), N_0 point to the initial density of neutral molecular in air, $N_{0,N_2} = 2\times10^{19}\text{cm}^{-3}$ and $N_{0,\text{O}_2} = 5\times10^{18}\ \text{cm}^{-3}$, respectively. R, I_T and α are empirical parameters used to fit the experimental data of ionization rate. Here, $R_{\text{N}_2} = 2.5\times10^4\ \text{s}^{-1}$, $R_{\text{O}_2} = 2.8\times10^6\ \text{s}^{-1}$, $I_T = 10^{13}\ \text{W/cm}^{-2}$, $\alpha_{\text{N}_2} \approx 7.5$, and $\alpha_{\text{O}_2} \approx 6.5$, respectively. Instead of the plasma

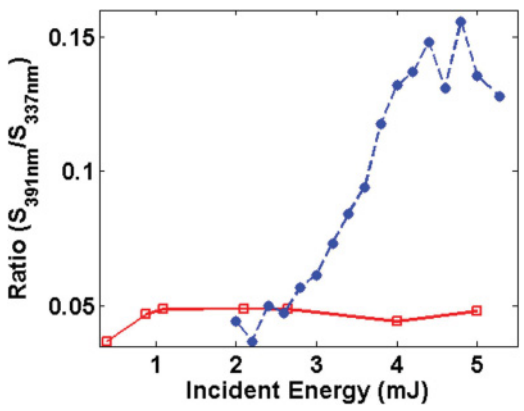

FIG. 5. (Color online) Experimentally measured intensity ratio of the 391-nm and the 337-nm lines as a function of the laser energy with (blue solid circles) and without (red open squares) using spatiotemporal focusing.

defocusing effect, the high-order Kerr effect (HOKE) has been recently proposed as an alternative mechanism to arrest the self-focusing [34,35]. The outcome parameters, including the clamped intensity, plasma density, filament length, and radius, are different quantitatively in two models [34–37]. Nevertheless, a counteracting nonlinear-process-induced intensity clamping phenomenon takes place in both models. Key aspects of the intensity clamping phenomenon with and without spatiotemporal focusing can be revealed as long as the comparison study is based on the same mechanism.

In simulations we have considered the propagation of a linearly polarized, collimated Gaussian input laser pulse with a central wavelength at $\lambda_0 = 800$ nm. In our simulation, the critical power for self-focusing was selected to be 10 GW in order to fit the previous experimental data [38]. The initial beam diameter is 5 mm ($1/e^2$). Note that a cylindrical symmetry coordinate was used in the simulation. Previous studies have demonstrated that a beam ellipticity will decrease the required power of multiple filamentation generation [39,40]. However, a single filament was generated in our experiment (see Fig. 2) eventually. Thereby, the spatial chirp evolution induced by the spatiotemporal focusing effect manifested mainly in the variation of the pulse duration. Previously, the effects of pulse chirping on the length and the duration of an atmospheric laser filament have been numerically examined by Nuter *et al.* [41]. According to Fig. 3, an effective GVD value of $k_2 = 1.1 \times 10^4$ fs^2/cm is implemented in our simulation. The corresponding input pulse duration is approximately 50 ps in the experiment. Because of this enormous value of GVD, laser peak intensity undergoes an abrupt change during propagation. For instance, when $z = 1.4$ mm the laser peak intensity is only half of the value at the focus in the case of linear propagation.

In the simulation of nonlinear propagation, the laser energy used is 1 mJ with initial diameter of 5 mm ($1/e^2$). The laser beam is focused by a $f = 100$ cm lens. The pulse duration is managed in such a way that it is chirp free at the focus in the case of linear propagation. Due to strong dispersion, the laser peak power reaches the critical power for self-focusing when $z = 1.4$ mm, which is already within the Rayleigh range ($\sim$3.9 cm) of the laser beam. Before $z = 1.4$ mm, the laser pulse is dominated by the linear propagation. Hence, for the sake of simplicity, it is reasonable to ignore the spatial chirp in the simulation, replaced by an effective value of k_2, especially when the distance approaches the focus. The obtained on-axis peak intensity was demonstrated in Fig. 6 as the solid line. Similar to the experimental result (Fig. 4), the laser intensity shows a steep increase before the focus and a fast decay when the distance exceeds the focus. The maximum intensity is higher than 10^{14} W/cm^2. The simulated corresponding spatiotemporal intensity distribution at geometric focus is depicted in Fig. 7(a). The laser energy is constrained within a narrow region of $\Delta\tau_{\mathrm{FWHM}} \approx 40$ fs and $\Delta d_{\mathrm{FWHM}} \approx 50$ μm. Due to self-steepening, the pulse is asymmetric in time. Furthermore, the simulated peak intensity as a function of the input laser energy when there was spatiotemporal focusing was depicted in Fig. 8 as the solid line. Intensity clamping takes place when the laser energy exceeds 1.5 mJ. The corresponding laser peak power is substantially higher than the critical power for self-focusing in air, which agrees well with the experimental observations as shown in Fig. 5.

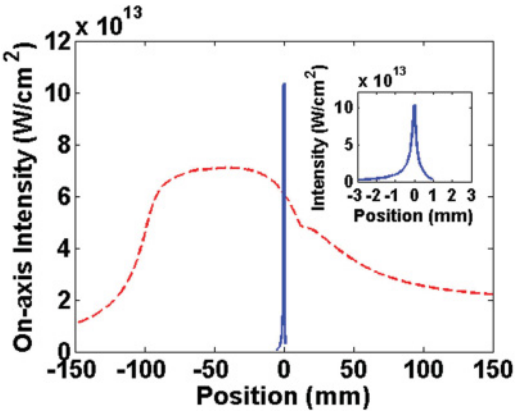

FIG. 6. (Color online) Calculated on-axis laser intensity as a function of the propagation distance with (solid line) and without (dashed line) using spatiotemporal focusing. Inset shows the solid line as an enlarged scale.

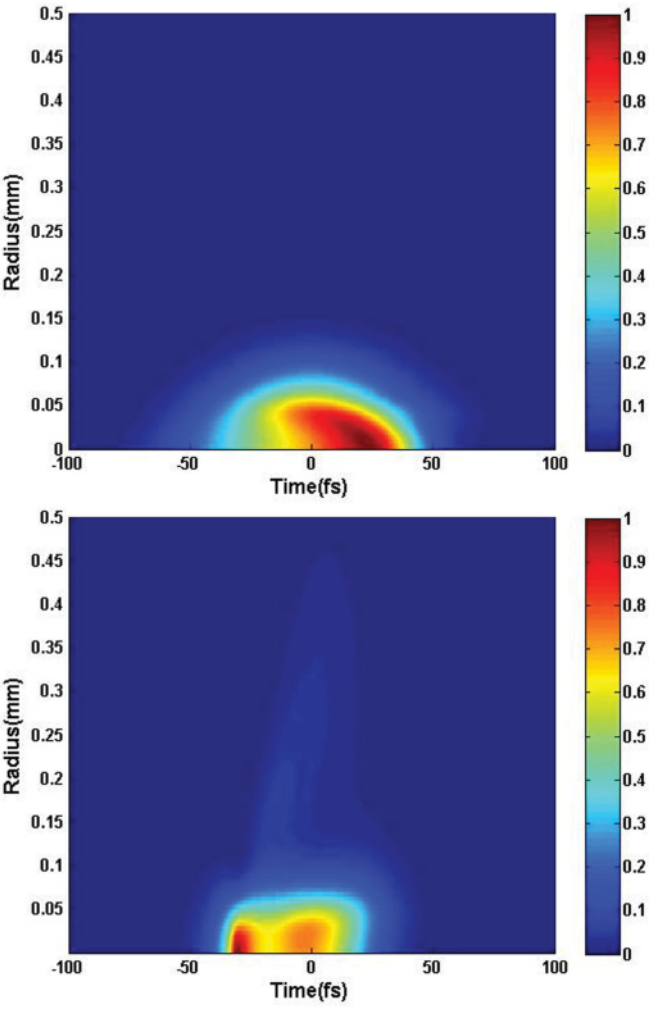

FIG. 7. (Color online) Simulated spatiotemporal intensity distribution at geometrical focus obtained (a) with and (b) without spatiotemporal focusing. Both panels are normalized to the maximum intensity.

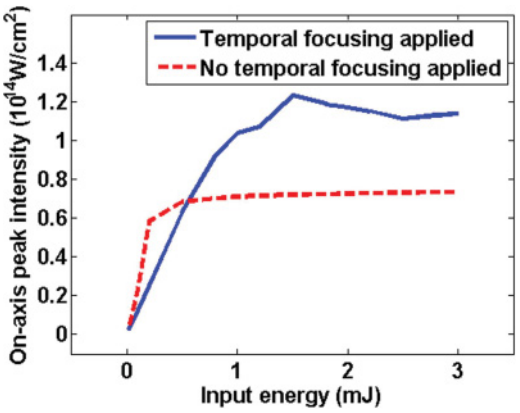

FIG. 8. (Color online) Simulated on-axis peak intensity as a function of the input laser energy with (solid line) and without (dashed line) using the spatiotemporal focusing technique.

As a comparison, the simulation on the basis of the standard model, in which no spatiotemporal focusing technique was implemented and $k_2 = 0.213$ fs^2/cm, has also been carried out. In this case, a transform-limited 40-fs laser pulse is directly focused by a $f = 100$ cm lens. The initial beam diameter and input laser energy are the same as those adopted in the simulation with spatiotemporal focusing, i.e., 5 mm ($1/e^2$) and 1 mJ, respectively. Therefore, the obtained on-axis laser intensity as a function of the propagation distance was depicted as the dashed line in Fig. 6, where peak intensity is about 7×10^{13} W/cm^2. This value is about two times lower than that when spatiotemporal focusing is used. The simulated spatiotemporal intensity distribution at geometric focus is present in Fig. 7(b). Unlike the spatiotemporal focusing case [Fig. 7(a)], though a short subpulse ($\Delta\tau_{\mathrm{FWHM}} \approx 10$ fs) is created in Fig. 7(b) due to the self-compression phenomenon [42–44], a large portion of the energy is widely distributed, constituting a background energy reservoir [31,45]. Consequently, the achieved peak intensity in Fig. 7(b) is less than that in Fig. 7(a). Pulse splitting is also clearly observed in Fig. 7(b) [46,47]. By using the same standard model, energy-dependent peak intensity was studied. The results are outlined in Fig. 8 as the dashed line. According to this plot, intensity clamping starts to play a dominant role when the critical power is reached, in agreement with the previous experiments [48].

It is worth emphasizing that in Ref. [48], various lenses with focal lengths ranging from 10 to 380 cm have been experimentally explored; the increase of laser intensity was constrained as long as the initial laser power exceeds the critical power for self-focusing. In contrast, our results (see Figs. 5 and 7) imply that by using spatiotemporal focusing, this intensity constraining point could be moved to a higher energy level, achieving enhanced laser intensity. The underlying physics could be understood as the outcome of the dynamic interplay between dispersion and nonlinear propagation as suggested by Ref. [41]. In our case, the control of the dynamics is realized by introducing an effective dispersion parameter via spatiotemporal focusing. On the other hand, in the conventional experimental scheme, to obtain higher laser intensity in the filament core, we can use a short focal length lens, but we cannot launch the filament far away in such case. However, through the spatiotemporal focusing technique, we can obtain higher laser intensity even at a far distance using a long focal length lens. For example, if using the same experimental configuration of spatiotemporal focusing, we simply increase the input laser energy to 40 mJ and change the focal length to 100 m. Then the laser peak power exceeds the critical power for self-focusing in air only when the propagation distance is further than 85 m according to our estimation. The filament will then start at a much longer distance, approaching the geometrical focus. Apparently it will prevent the early development of filamentation which is the main obstacle for projecting filament to a remote distance. In this sense, the spatiotemporal focusing technique demonstrated here somehow achieves the same goal as the previously reported telescope technique [49,50], but with focal lenses of much smaller apertures.

V. CONCLUSION

In conclusion, we have shown that by employing the spatiotemporal focusing technique, the peak intensity in the filamentation core can be effectively enhanced as compared to that allowed by a loose focusing geometry. In addition, the filamentation length is significantly shortened as a result of elongated pulse duration in the out-of-focus region. The numerical simulations reproduce the experimental results fairly well. Our result could be of great interest in remote sensing for achieving better spatial (longitudinal) resolution and high signal-to-noise ratio while keeping the flexibility of being able to project the filament at long distances. This technique can also be useful for other important applications, such as high-order harmonic generation. Higher conversion efficiency and higher cutoff photon energies could be attainable due to the higher achievable peak intensity gained from the temporal focusing technique.

ACKNOWLEDGMENTS

This research is financially supported by National Basic Research Program of China (Grant No. 2011CB808100), and National Natural Science Foundation of China (Grants No. 10974213, No. 10804056, No. 60825406, and No. 11174156). S.L.C. is supported by the Canada Research Chair.

[1] S. L. Chin, S. A. Hosseini, W. Liu, Q. Luo, F. Théberge, N. Aközbek, A. Becker, V. P. Kandidov, O. G. Kosareva, and H. Schroeder, Can. J. Phys. **83**, 863 (2005).
[2] A. Couairon and A. Mysyrowicz, Phys. Rep. **441**, 47 (2007).
[3] L. Bergé, S. Skupin, R. Nuter, J. Kasparian, and J.-P. Wolf, Rep. Prog. Phys. **70**, 1633 (2007).
[4] J. Kasparian and J.-P. Wolf, Opt. Express **16**, 466 (2008).
[5] S. L. Chin, *Femtosecond Laser Filamentation* (Springer Science + Business Media, New York, 2010).
[6] V. P. Kandidov, S. A. Shlenov, and O. G. Kosareva, Quantum Electron. **39**, 205 (2009).

[7] B. La Fontaine, F. Vidal, Z. Jiang, C. Y. Chien, D. Comtois, A. Desparois, T. W. Johnston, J. C. Kieffer, H. Pepin, and H. P. Mercure, Phys. Plasmas **6**, 1615 (1999).
[8] G. Méchain *et al.*, Appl. Phys. B: Lasers Opt. **80**, 785 (2005).
[9] J. Kasparian *et al.*, Science **301**, 61 (2003).
[10] A. Braun, G. Korn, X. Liu, D. Du, J. Squier, and G. Mourou, Opt. Lett. **20**, 73 (1995).
[11] J. Bernhardt, W. Liu, S. L. Chin, and R. Sauerbrey, Appl. Phys. B: Lasers Opt. **91**, 45 (2008).
[12] O. G. Kosareva *et al.*, Laser Phys. **19**, 1776 (2009).
[13] J. Kasparian, R. Sauerbrey, and S. L. Chin, Appl. Phys. B: Lasers Opt. **71**, 877 (2000).
[14] A. Becker, N. Aközbek, K. Vijayalakshmi, E. Oral, C. M. Bowden, and S. L. Chin, Appl. Phys. B: Lasers Opt. **73**, 287 (2001).
[15] W. Liu, S. Petit, A. Becker, N. Aközbek, C. M. Bowden, and S. L. Chin, Opt. Commun. **202**, 189 (2002).
[16] F. Théberge, N. Aközbek, W. Liu, A. Becker, and S. L. Chin, Phys. Rev. Lett. **97**, 023904 (2006).
[17] X.-L. Liu, X. Lu, X. Liu, T.-T. Xi, F. Liu, J.-L. Ma, and J. Zhang, Opt. Express **18**, 26007 (2010).
[18] P. P. Kiran, S. Bagchi, C. L. Arnold, S. R. Krishnan, G. R. Kumar, and A. Couairon, Opt. Express **18**, 21504 (2010).
[19] F. He, H. Xu, Y. Cheng, J. Ni, H. Xiong, Z. Xu, K. Sugioka, and K. Midorikawa, Opt. Lett. **35**, 1106 (2010).
[20] E. Takahashi, Y. Nabekawa, T. Otsuka, M. Obara, and K. Midorikawa, Phys. Rev. A **66**, 021802 (2002).
[21] G. P. Agrawal, *Nonlinear Fiber Optics*, 4th ed. (Academic Press, New York, 2007).
[22] A. Talebpour, M. Abdel-Fattah, A. D. Bandrauk, and S. L. Chin, Laser Phys. **11**, 68 (2001).
[23] A. Becker, A. D. Bandrauk, and S. L. Chin, Chem. Phys. Lett. **343**, 345 (2001).
[24] A. Talebpour, J. Yang, and S. L. Chin, Opt. Commun. **163**, 29 (1999).
[25] H. L. Xu, A. Azarm, J. Bernhardt, Y. Kamali, and S. L. Chin, Chem. Phys. **360**, 171 (2009).
[26] V. P. Kandidov, O. G. Kosareva, I. S. Golubtsov, W. Liu, A. Becker, N. Akozbek, C. M. Bowden, and S. L. Chin, Appl. Phys. B: Lasers Opt. **77**, 149 (2003).
[27] T. Brabec and F. Krausz, Phys. Rev. Lett. **78**, 3282 (1997).
[28] A. Couairon, M. Franco, A. Mysyrowicz, J. Biegert, and U. Keller, Opt. Lett. **30**, 2657 (2005).
[29] H. S. Chakraborty, M. B. Gaarde, and A. Couairon, Opt. Lett. **31**, 3662 (2006).
[30] L. Bergé, Opt. Express **16**, 21529 (2008).
[31] M. Mlejnek, E. M. Wright, and J. V. Moloney, Opt. Lett. **23**, 382 (1998).
[32] A. Chiron, B. Lamouroux, R. Lange, J. F. Ripoche, M. Franco, B. Prade, G. Bonnaud, G. Riazuelo, and A. Mysyrowicz, Euro. Phys. J. D: At. Mol. Opt. Plasma Phys. **6**, 383 (1999).
[33] J.-F. Ripoche, G. Grillon, B. Prade, M. Franco, E. Nibbering, R. Lange, and A. Mysyrowicz, Opt. Commun. **135**, 310 (1997).
[34] P. Bejot, J. Kasparian, S. Henin, V. Loriot, T. Vieillard, E. Hertz, O. Faucher, B. Lavorel, and J. P. Wolf, Phys. Rev. Lett. **104**, 103903 (2010).
[35] P. Béjot, E. Hertz, J. Kasparian, B. Lavorel, J. P. Wolf, and O. Faucher, Phys. Rev. Lett. **106**, 243902 (2011).
[36] M. Kolesik, D. Mirell, J. C. Diels, and J. V. Moloney, Opt. Lett. **35**, 3685 (2010).
[37] P. Polynkin, M. Kolesik, E. M. Wright, and J. V. Moloney, Phys. Rev. Lett. **106**, 153902 (2011).
[38] W. Liu and S. Chin, Opt. Express **13**, 5750 (2005).
[39] A. Dubietis, G. Tamošauskas, G. Fibich, and B. Ilan, Opt. Lett. **29**, 1126 (2004).
[40] T. Grow and A. Gaeta, Opt. Express **13**, 4594 (2005).
[41] R. Nuter, S. Skupin, and L. Bergé, Opt. Lett. **30**, 917 (2005).
[42] C. P. Hauri, W. Kornelis, F. W. Helbing, A. Heinrich, A. Couairon, A. Mysyrowicz, J. Biegert, and U. Keller, Appl. Phys. B: Lasers Opt. **79**, 673 (2004).
[43] G. Stibenz, N. Zhavoronkov, and G. Steinmeyer, Opt. Lett. **31**, 274 (2006).
[44] L. Bergé and S. Skupin, Phys. Rev. Lett. **100**, 113902 (2008).
[45] W. Liu, F. Théberge, E. Arévalo, J. F. Gravel, A. Becker, and S. L. Chin, Opt. Lett. **30**, 2602 (2005).
[46] A. L. Gaeta, Phys. Rev. Lett. **84**, 3582 (2000).
[47] S. A. Diddams, H. K. Eaton, A. A. Zozulya, and T. S. Clement, Opt. Lett. **23**, 379 (1998).
[48] F. Théberge, W. Liu, P. T. Simard, A. Becker, and S. L. Chin, Phys. Rev. E **74**, 036406 (2006).
[49] W. Liu, F. Théberge, J. F. Daigle, P. T. Simard, S. M. Sarifi, Y. Kamali, H. L. Xu, and S. L. Chin, Appl. Phys. B: Lasers Opt. **85**, 55 (2006).
[50] S. Eisenmann, E. Louzon, Y. Katzir, T. Palchan, A. Zigler, Y. Sivan, and G. Fibich, Opt. Express **15**, 2779 (2007).